Sensors and Actuators A 286 (2019) 4–13

Contents lists available at ScienceDirect

Sensors and Actuators A: Physical

journal homepage: www.elsevier.com/locate/sna

Material and device design for the high performance low temperature co-fired multilayer piezoelectric transformer

Sinan Dursun[a,*], Ahmet Erkan Gurdal[b], Safakcan Tuncdemir[b], Clive Randall[a]

[a] Materials Research Institute and Materials Science and Engineering Department, The Pennsylvania State University, University Park, PA 16802, United States

[b] Solid State Ceramics, Inc., 341 Science Park Road., Suite 105, State College, PA 16803 United States

ARTICLE INFO

Article history:
Received 17 May 2018
Received in revised form
19 November 2018
Accepted 14 December 2018
Available online 15 December 2018

Keywords:
Multilayer
Piezoelectric transformer
Low temperature co-firing
High power
Hard piezoelectric ceramics

ABSTRACT

PZT-based perovskite structure relaxors are very attractive for high power piezoelectric applications. Targeting multilayer co-fired piezoelectric transformers, we developed a PNN-PMW-PZT system [$Pb(Ni_{1/3}Nb_{2/3})O_3$-$Pb(Mg_{1/2}W_{1/2})O_3$-$0.9Pb(Zr_{0.5}Ti_{0.5})O_3$+x$MnO_2$] and used flux materials to decrease the sintering temperature. Systematically investigating the effect of MnO_2 content on piezoelectric and dielectric properties, the composition with 0.25 wt% MnO_2 hardener exhibited excellent piezoelectric properties after sintering at 1000 °C for 2 h (Q_m: 1150, k_p: 0.63, d_{33}: 345, tan δ: 0.0040, $\varepsilon^T_{33}/\varepsilon_0$: 1030). In addition to the compositional development, this work also involved functional tests and high-power characterization of a multilayer piezoelectric transformer utilizing this new ternary system that provided 38 W/cm^3 output power density with 92% efficiency and a step-up ratio of 7.

1. Introduction

Piezoelectric transformers (PT) are capacitive energy transfer devices where the electrical energy is converted to acoustic energy at input section, and the acoustic energy is simultaneously converted back to electrical energy at output section. Although piezoelectric ceramics have been widely used as actuators, transducers, and sensors, the only relevant application of piezoelectric transformers was limited to the backlight inverters in LCD displays for portable devices [1]. The narrow commercial application field of PT is mainly attributed to its high cost per unit power; it can handle at high efficiency compared to the legacy electromagnetic transformers (EMT).However, there is a growing interest for PTs from the defense and space industry, considering their higher operating temperature, fast charging, and high potential step-up capability compared to EMTs, in addition to their radiation inertness and immunity to electromagnetic interference, which reduces the burden of shielding in radiation-exposed and extreme environment applications.

There have been two critical approaches that have to be considered simultaneously to improve the power handling capability of PTs. First is to optimize hard-type piezoceramic materials used in PTs to decrease material losses and enhance coupling at high vibration velocity, and thus improve efficiency and power handling capacity of PTs [2]. The second approach is to implement co-fired multilayering to increase power density of PT [3,4]. As shown in our previous paper [5], the latter approach increases the cost of PT significantly, unless cost-effective Ag-alloys or Cu can replace high-cost Pt as inner-layer electrodes, which is challenging because sintering temperature of hard-type piezoceramics are typically too high (>1100 °C) to be applicable for co-firing with Ag-alloys and Cu. Therefore, the aim of this study is to develop new hard-type material that has low sintering temperature enabling base metal electrode co-firing and still possesses desirable material properties (high Q_m, k_p, d_{33}, and low dielectric loss) for high-performance PT.

Conventionally, PTs are built from hard-type piezoceramics because of their high mechanical quality factor (Q_m) and low dielectric losses (tan δ). High electromechanical coupling (k_p, k_t), piezoelectric response (d_{33}), and Curie temperature are also desired material parameters [2]. Due to their high piezoelectric coefficients (d_{33}), large electromechanical coupling factors (k_p), and high mechanical quality factors (Q_m), Pb $\boldsymbol{B'B''}$ O_3–PZT-based ferroelectric ceramic compositions have been widely investigated. Although the majority of literature on the low temperature sintering binary,

* Corresponding author at: Materials Research Institute, N249 Millennium Science Complex, The Pennsylvania State University, University Park, PA 16802, United States.
E-mail address: sxd448@psu.edu (S. Dursun).

https://doi.org/10.1016/j.sna.2018.12.017
0924-4247/

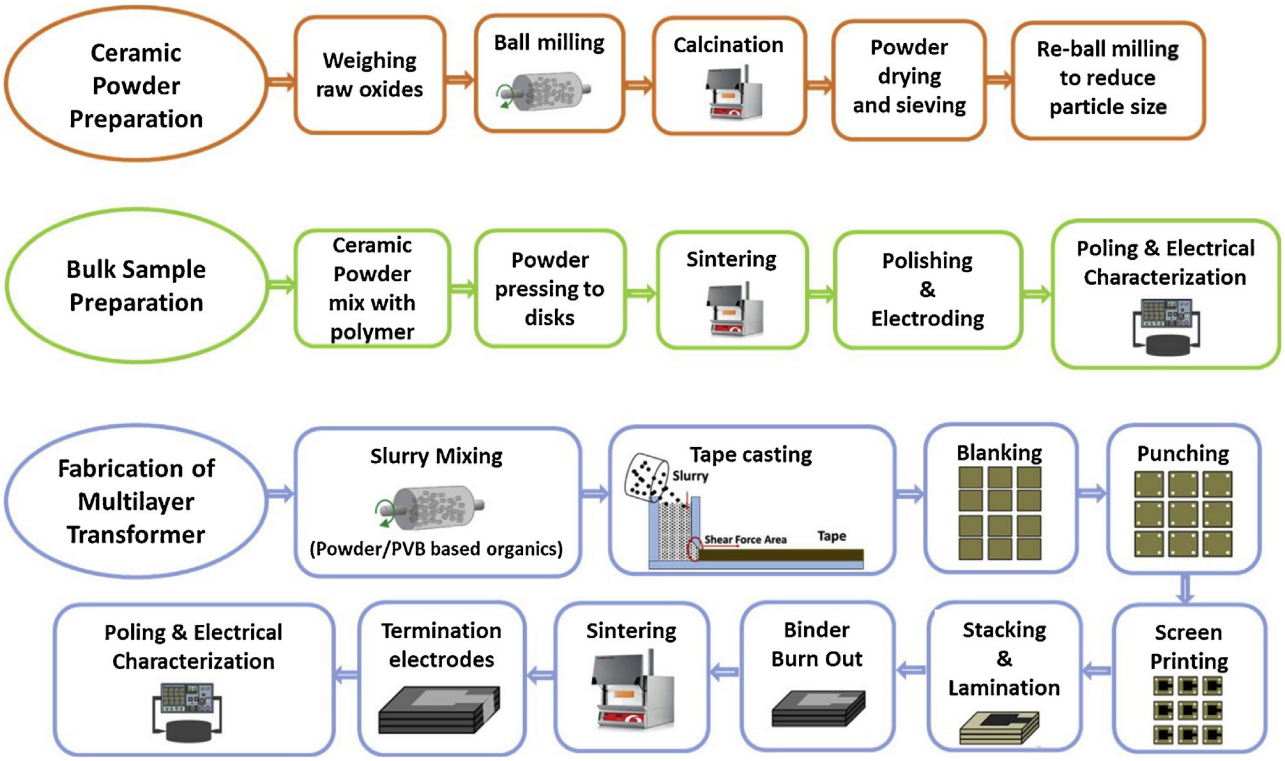

Fig. 1. Simplified schematic representations of ceramic powder processing, bulk sample preparation and fabrication of multilayer transformer.

ternary, and quaternary Pb(B'B")O_3 – PZT solid solutions are targeting multilayer actuators due to large piezoelectric response (d_{33}), there are also notable studies that report promising hard-type properties achieved at low temperature sintering. S. Y. Yoo et al. [6] studied a PMN-PAN-PZT system, in which La_2O_3 was used as an acceptor dopant (hardening), and CuO was used as a flux to enable low temperature (900 °C, 2 h) sintering, and exhibited favorable electrical and electromechanical properties (d_{33} = 336 pC/N, Q_m = 841, and k_p = 0.60) for high power applications. D. Wan et al. [7] used similar hardener and flux agent in a 900 °C (4 h) sintered PZT-PMS-PZN system that provided promising high-power properties (d_{33} = 355 pC/N, Q_m = 936, k_p = 0.58). J. Yoo et al. [8] developed a 900 °C sintered PMnN-PNN-PZT composition, which utilized Li_2CO_3 and Na_2CO_3 as sintering aids and MnO_2 as hardener, and exhibited electrical properties (d_{33} = 356 pC/N, k_p = 0.6, and Q_m = 1186) suitable for co-fired structures for high-power applications. In addition to the large mechanical quality factor (Q_m>1000), and high piezoelectric response (d_{33}~350 pC/N), the dielectric loss in piezoelectric transformer materials should be low (<0.004) in order to prevent heat generation under high field drive conditions and hence to improve the power density. Furthermore, piezoelectric transformer applications also require high electromechanical coupling factor (k_p>0.60) to improve power efficiency and the operating bandwidth of the devices. The previously reported low-sintering temperature hard compositions do not meet the combination of these properties that further improve the power handling limits of piezoelectric transformers. In order to fill this gap, this study aims to develop a high-performance low-sintering temperature piezoelectric transformer material.

A recently reported PNN-PMW-PZT composition is selected as the starting system because of its excellent soft properties (d_{33} = 599 pC/N, k_p = 0.7, Q_m = 50, T_C = 296 °C, and ε^T_{33} = 2595) [9]. To obtain optimum hard-type properties, as to improve Q_m and to decrease dielectric losses of this very prominent soft-type composition, MnO_2 is chosen as the hardening dopant, while $CaCO_3$ and Li_2O_3 are employed for low temperature sintering. The comprehensive developmental report of the hard-type low temperature sinterable PNN-PMW-PZT piezoceramic composition [$Pb(Ni_{1/3}Nb_{2/3})O_3$-$Pb(Mg_{1/2}W_{1/2})O_3$-0.9$Pb(Zr_{0.50}Ti_{0.50})O_3$]+x$MnO_2$] provided in subsequent sections includes the systematic investigation of the effect of MnO_2 content and sintering temperature on piezoelectric and dielectric properties. In order to demonstrate the very high figure-of-merit of the developed PNN-PMW-PZT piezoceramic composition, a ring-dot step-up multilayer piezoelectric transformer co-fired with Ag/Pd electrodes was built, and the comprehensive details of the device microstructure and performance were provided subsequent sections.

2. Experimental procedure

2.1. Ceramic powder and bulk sample preparation

The 0.08$Pb(Ni_{1/3}Nb_{2/3})O_3$-0.02$Pb(Mg_{1/2}W_{1/2})O_3$-0.90$Pb(Zr_{0.50}Ti_{0.50})O_3$-x$MnO_2$:[PNN-PMW-PZT-Mn] composition was fabricated using a conventional mixed oxide process with different amounts of MnO_2 content, where x = 0.1, 0.25 and 0.5 wt% and with sintering aids Li_2O_3 and $CaCO_3$, 0.2 wt% and 0.3 wt%, respectively [9]. Fig. 1 depicts the schematic representation of the bulk and multilayer sample preparation. Raw oxides and carbonates PbO (Alfa Aesar, 99.5%), MgO (Alfa Aesar, 99%), WO_3 (Alfa Aesar, 99%), NiO (Alfa Aesar, 99%), Nb_2O_5 (Alfa Aesar, 99.5%), ZrO_2 (Alfa Aesar, 99%), TiO_2 (Alfa Aesar, 99%), Li_2CO_3 (Alfa Aesar, 99%), and $CaCO_3$ (Alfa Aesar, 99%), MnO_2(Alfa Aesar, 99%) were weighted by molar ratio according to the chemical formula and mixed by ball mill with YSZ in Et-OH for 24 h. The mixed powders were calcined at 780 °C for 4 h and ball milled for 24 h again to decrease particle size and eliminate the agglomerates. After that, dried powder was mixed with 1.5 wt% Paraloid in acetone solution with ball mill for 6 h. Then, powder was sieved and uniaxially pressed into disks

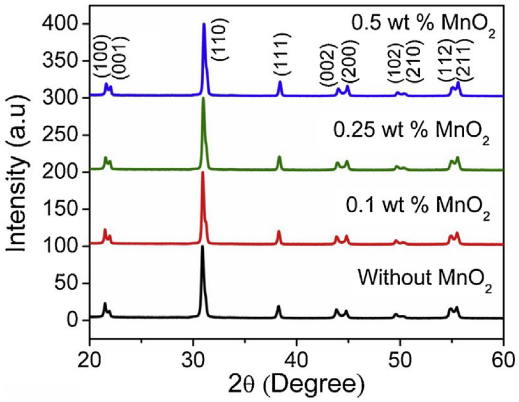

Fig. 2. The X-ray diffraction patterns of PNN-PMW-PZT as a function of MnO_2 doped.

shape pellets with diameter of 12.5 mm. Binder burn-out was performed at 550 °C for 2 h to remove the polymer binder, and then the samples were sintered in the range of 900–1100 °C for 2 h. Sintered disks were polished and printed with Ag (Heraeus, C8829 A) electrode and then fired at 590 °C for 15 min. Fired piezoceramics were poled in silicone oil at 120 °C under an electric field of 3 kV/mm for 15 min. The poled ceramics were then aged for 24 h before the final electrical characterizations.

2.2. Fabrication of multilayer -LTCC

The details of multilayer co-fired process was provided in our previous paper [5]. The sintering of multilayer PNN-PMW-PZT samples was performed at 1000 °C for 2 h with covered alumina crucible. Terminals of the transformers were polished to expose the electrodes and then terminated with Ag (Heraeus, C8829 A) termination electrode at 490 °C for 15 min. Then input and output sections were poled separately according to their individual ceramic thicknesses and thus poling fields.

2.3. Material and electrical characterization

Phase and microstructure analysis of bulk sample were carried out with X-ray diffraction (PANalytical Empyrean X-Ray Diffractometer), scanning electron micrographs (SEM) and EDS mapping (FEI Nova NanoSEM 630 SEM). The room temperature dielectric loss and capacitance of ceramics and PTs were measured at 1 kHz and 1 V with an LCR meter (HP 4772 A, LCR meter). The piezoelectric charge coefficient (d_{33}) of poled ceramics was measured at 100 Hz under 10 N force with a Berlincourt type d_{33} meter. Planar electromechanical coupling coefficient (k_p) and mechanical quality factor (Q_m) were calculated according to IEEE standards from impedance spectra which was recorded by an impedance analyzer (HP-4294 A, Impedance analyzer). After completing necessary characterization, PT devices were characterized with an oscilloscope and probes to investigate high voltage step-up capabilities.

3. Result and discussion

3.1. Phase and microstructure analysis

Fig. 2 shows the X-ray diffraction (XRD) patterns of PNN-PMW-PZT $(0.08Pb(Ni_{1/3}Nb_{2/3})O_3\text{-}0.02Pb(Mg_{1/2}W_{1/2})O_3\text{-}0.90Pb(Zr_{0.50}Ti_{0.50})O_3$ disk sample with and without MnO_2 dopant sintered at 1000 °C for 2 h. The samples showed a pure perovskite structure with an apparent (002)/(200) peak splitting, which confirms the tetragonal crystal structure. XRD patterns also showed that MnO_2 content does not influence the phase structure.

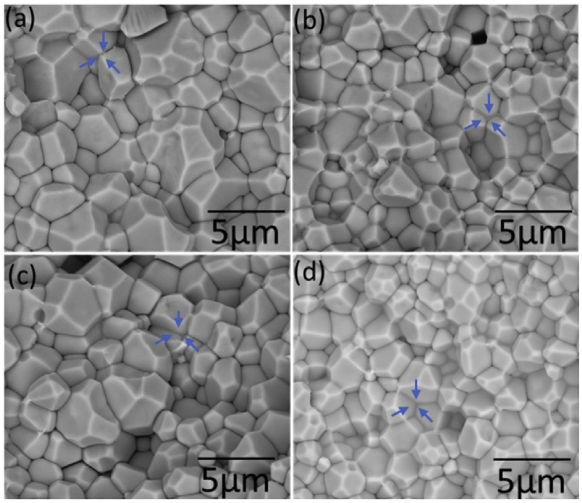

Fig. 3. Microstructure of fracture surface PNN-PMW-PZT ceramics with/without Mn-doped sintered at 1000 °C for 2 h: (a) 0, (b) 0.1, (c) 0.25, (d) 0.5.

As already reported, the second phase compounds like Li_2PbO_3 that are observed on the surface of 0.08PNN-0.02PMW-0.9PZT ceramics are attributed to the Li_2CO_3 content exceeding the limit of solubility [9,10]. Therefore, the amount of $LiCO_3$ is limited with 0.2 wt% for this study, where no secondary phases are observed. The XRD of calcined powder exhibit rhombohedral and tetragonal phases coexisting in MnO_2 doped calcined powder (not shown here); however, after sintering, the crystal structure changed to tetragonal phase.

Fig. 3 presents SEM micrographs of a cross-sectional fracture surface of undoped and doped PNN-PMW-PZT ceramics sintered at 1000 °C for 2 h. There is no secondary phase or segregation observed in PNN-PMW-PZT ceramics via SEM micrographs. The results were confirmed by XRD patterns of these ceramics (see Fig. 2). The grain size of the PNN-PMW-PZT ceramics with doped and undoped MnO_2 were analyzed from fractured surface of SEM images by a line intersect method. Undoped and 0.25 wt% MnO_2 doped PNN-PMW-PZT ceramics samples are shown in Fig. 3 (a) and (c), revealing inhomogeneous grain size distributions ranging from 5.60 μm to 2.30 μm. The average grain size of the undoped and 0.25 wt% MnO_2 doped ceramics were calculated to be 2.57 μm and 2.50 μm, respectively. However, the grain size distribution was uniform for both 0.1 wt% and 0.5 wt% MnO_2 doped samples with 2.10 μm and 2.05 μm, respectively.

Liquid phase sintering is a well-known process that is carried out significantly below the conventional sintering temperature due to the eutectic point of that mixed metal oxides powder (i.e. Li_2O_3, CuO, PbO) with ceramic powder [11,12]. In this study, we used Li_2CO_3 as sintering aid that reacts with PbO to form liquid phase with a low melting point of 836 °C [13]. Liquid phase sintering leads to rapid densification and shrinkage of PNN-PMW-PZT ceramics due to particle re-arrangement at initial stages of sintering. During cooling, the liquid phase forms around the grain boundaries, as indicated in Fig. 3. In addition, it is well known that MnO_2 significantly influences the density when MnO_2 is added to PZT-based ceramics without exceeding the solubility limit; Mn ions homogeneously dissolve in the perovskite structure and enhance the densification of the ceramics [14]. The effect of MnO_2 doping on the density was measured with the Archimedes method in DI water. The density of PNN-PMW-PZT sample without MnO_2 doping was measured 7.80 g/cm^3 and stayed almost same (7.79 g/cm^3) with 0.1 wt% MnO_2 doping. Further increase of MnO_2 doping to 0.25 wt% and 0.5 wt% increased relative density of the bulk samples to 7.90 g/cm^3 and 7.95 g/cm^3, respectively.

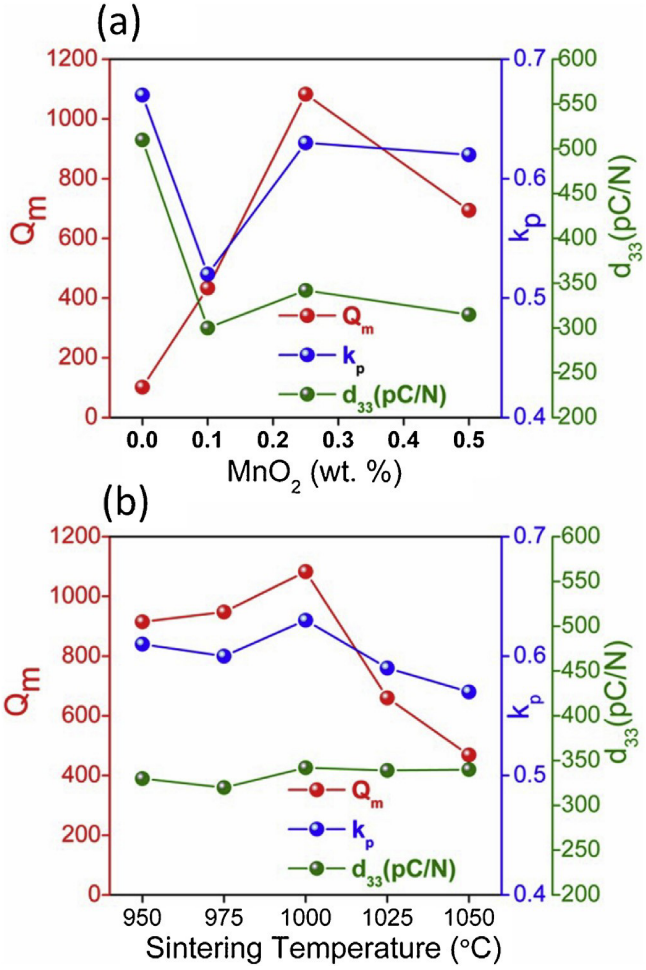

Fig. 4. Electromechanical and piezoelectric properties of PNN-PMW-PZT as a function of MnO_2 content sintered at 1000 °C for 6 h (a) and PNN-PMW-PZT with 0.25 wt% MnO_2 as a function of sintering temperature (b).

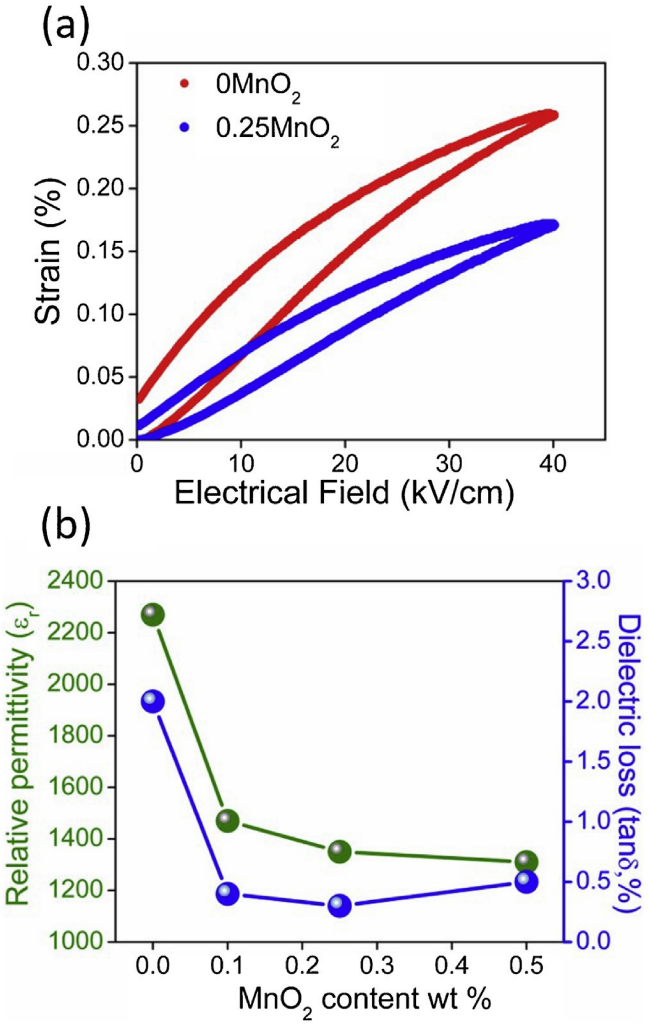

Fig. 5. Unipolar strain curves (x-E) were measured from PNN-PMW-PZT ceramics with 0.25 wt% doped MnO_2 and undoped sintered at 1000 °C for 2 h (a), and Relative permittivity (ε_r) and dielectric loss (tan δ, %) of PNN-PMW-PZT with different MnO_2 (b).

3.2. Electrical and electromechanical characterization

Electromechanical and piezoelectric properties of PNN-PMW-PZT measured as a function of MnO_2 content and sintering temperature were given in Fig. 4. As seen in Fig. 4a, the addition of 0.1 wt% MnO_2 increased the mechanical quality factor (Q_m) significantly, whereas decreased the coupling coefficient (k_p) and piezoelectric strain coefficient (d_{33}) are due to the hardening effect. The hardening effect of MnO_2 was explained by stabilization of domain structure [14]. According to this assumption, the manganese ion acts as an acceptor dopant and can ionically compensate to create oxygen vacancies in the crystal lattice. The coexisting Mn^{2+} and Mn^{3+} ions in perovskite PZT structure can easily dissolve to substitute preferentially occupied B-site or octahedral ions (Zr^{4+}, Ti^{4+}) [8,13]. Mn ions that occupy the lower valances site create oxygen vacancies to maintain bulk, as given below:

$$Mn^{3+} \rightarrow Mn'_{Zr,Ti} + \frac{1}{2}V_{o}^{\cdot\cdot} \quad (1)$$

$$Mn^{2+} \rightarrow Mn''_{Zr,Ti} + V_{o}^{\cdot\cdot} \quad (2)$$

Acceptor ions and oxygen vacancies lead to defect dipoles and/or distributed defect dipoles, and these defects act as pinning points for the ferroelectric and ferroelastic domain motion/mobility, which was pinned by defect dipoles by means of internal electrical field [15]. In addition, the change in grain size directly influenced the piezoelectric properties. Coarser grain size ceramics showed larger d_{33} and k_p, as previously observed by H. Du et al. and C. Randall [16,17]. The increase in d_{33} and k_p was attributed to the grain size increase when MnO_2 was 0.25 wt%. As provided in Fig. 4(b), sintering temperature dependence of piezoelectric properties was investigated, and the optimum properties were achieved at 1000 °C also enabling Ag/Pd co-firing with low Pd contents and, very importantly, opened up the possibility of Cu co-firing. This topic will be covered in a future report, separately. At this sintering temperature, 0.25 wt% MnO_2 doped PNN-PMW-PZT ceramics exhibited excellent hard electromechanical properties of d_{33} = 350 pC/N, k_p = 0.63, and Q_m = 1150. These measured values are well suited for high power applications, and specifically for ceramic transformers.

Fig. 5 (a) shows the unipolar strain curves (x-E) of undoped and doped PNN-PMW-PZT ceramics as a function of electrical field, which was applied at room temperature in silicone oil. Samples are sintered at 1000C° for 2 h and poled under 3 kV/mm at 120 °C for 15 min. Undoped PNN-PMW-PZT ceramics show higher strain than 0.25 wt% MnO_2 doped ceramics, which is attributed to the soft piezoelectric properties due to the domain wall motion. The piezoelectric coefficient of the doped and undoped PNN-PMW-PZT ceramics is calculated to be 645 pC/N and 425 pC/N, respectively from the high field unipolar strain curve; whereas the Berlincourt measurements provide 540 pC/N and 368 pC/N due to the absence

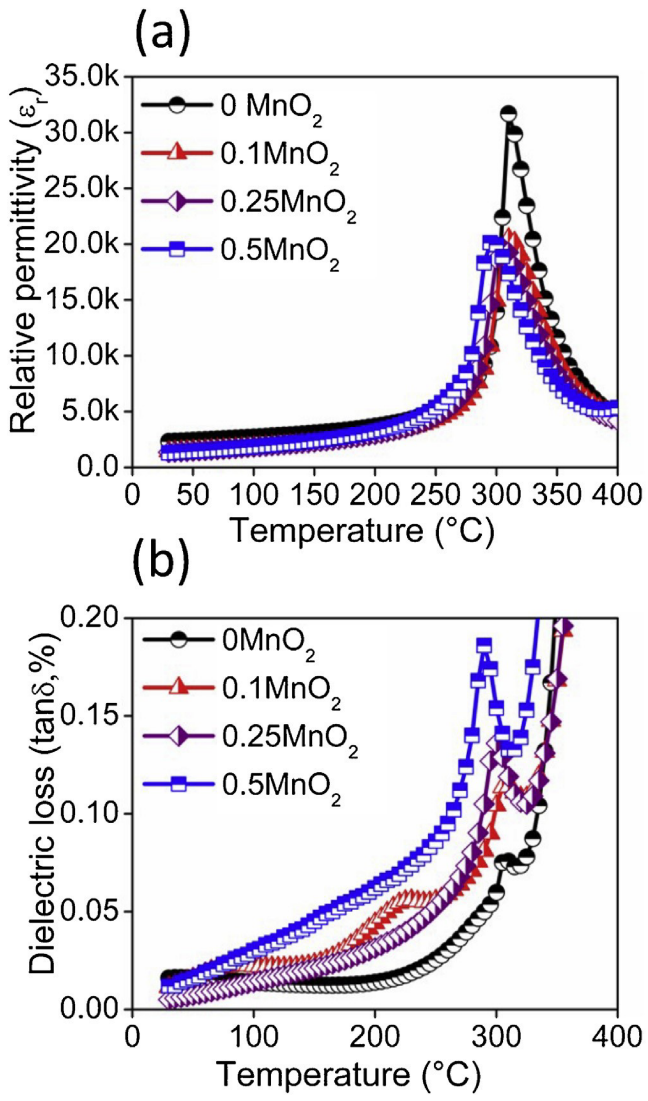

Fig. 6. The relative permittivity (a) and dielectric loss (tan δ, %) (b) of PNN-PMW-PZT as a function of temperature according to the variation of amount MnO_2 doped.

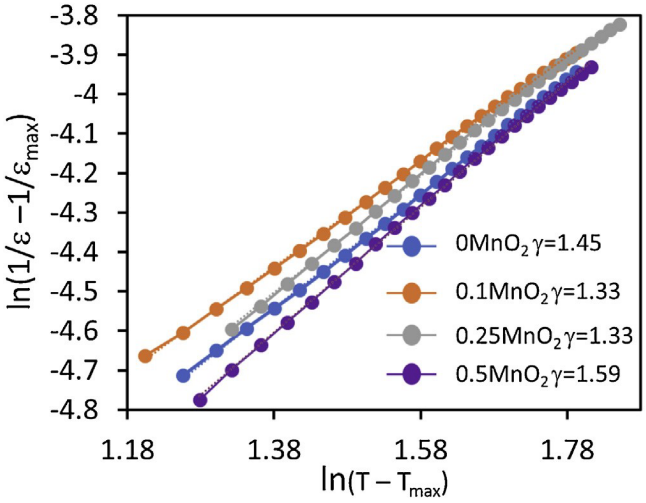

Fig. 7. ln $(1/\varepsilon - 1/\varepsilon_{max})$ versus **ln**$(T - T_{max})$ for the PNN-PMW-PZT ceramics with different MnO_2 doping.

of the extrinsic domain wall contribution under the higher fields [18]. The relative permittivity and dielectric loss properties of PNN-PMW-PZT piezoceramics were investigated as a function of dopant content and temperature. Typical to a soft piezo ceramic, undoped PNN-PMW-PZT has high dielectric loss and relative permittivity; however, with the increase of Mn, loss and dielectric constant decrease, which represents hardening effect (Fig. 5(b)) [19,20].

Analyzing the temperature dependence of the relative permittivity and dielectric loss, the Curie Temperature (T_C) was measured as 310 °C for undoped and 295 °C for MnO_2 doped PNN-PMW-PZT ceramics (Fig. 6). It is also interesting to note that undoped composition has higher relative permittivity at T_C. While undoped PNN-PMW-PZT ceramic has sharp and narrow ferroelectric-paraelectric phase transition, doped ceramics have more broad phase transition with typical behaviour relaxor $Pb(B'B'')O_3$ - PZT solid solutions. Curie-Weiss law describes the diffuse phase transition in relaxor ferroelectrics with diflux permittivity peaks and is given as Formula 3 [21], where K is the dielectric constant at T, K_{max} is the maximum value of the dielectric constant at T_{max}, γ is the degree of diffuseness (or degree of dielectric relaxation in relaxor ferroelectric material), and C is a constant. γ is a key parameter for a ferroelectric system to define as normal ferroelectric and relaxor ferroelectric.

$$\frac{1}{K} = \left(\frac{1}{K_{max}}\right) + \frac{[(T - T_{max})^{\gamma}]}{C} \quad (3)$$

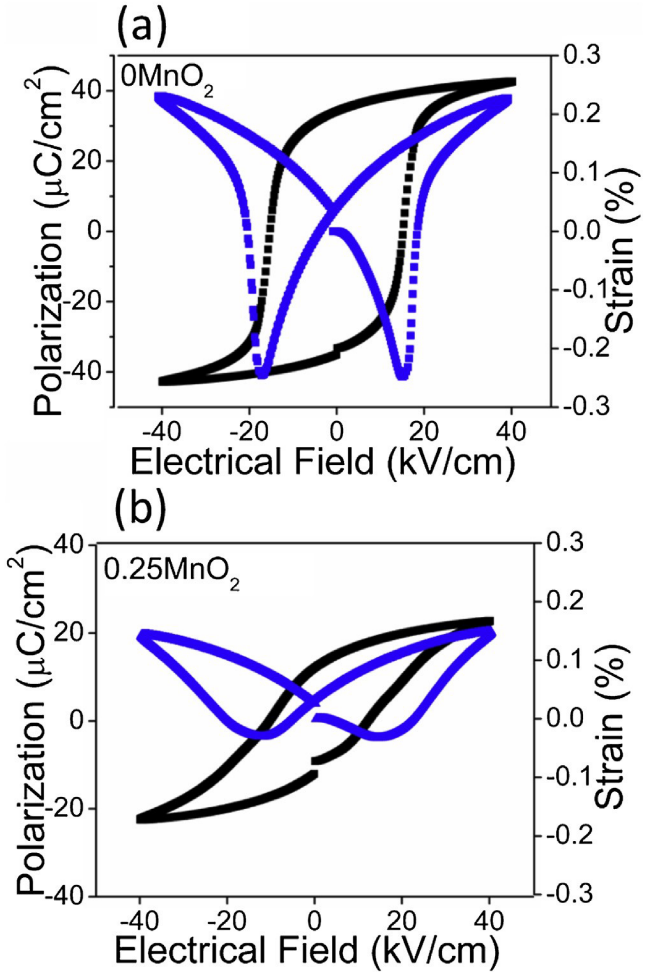

Fig. 8. Electrical field induced polarization (P-E) and bipolar strain (x-E) hysteresis of (a) undoped and (b) doped PNN-PMW-PZT ceramics.

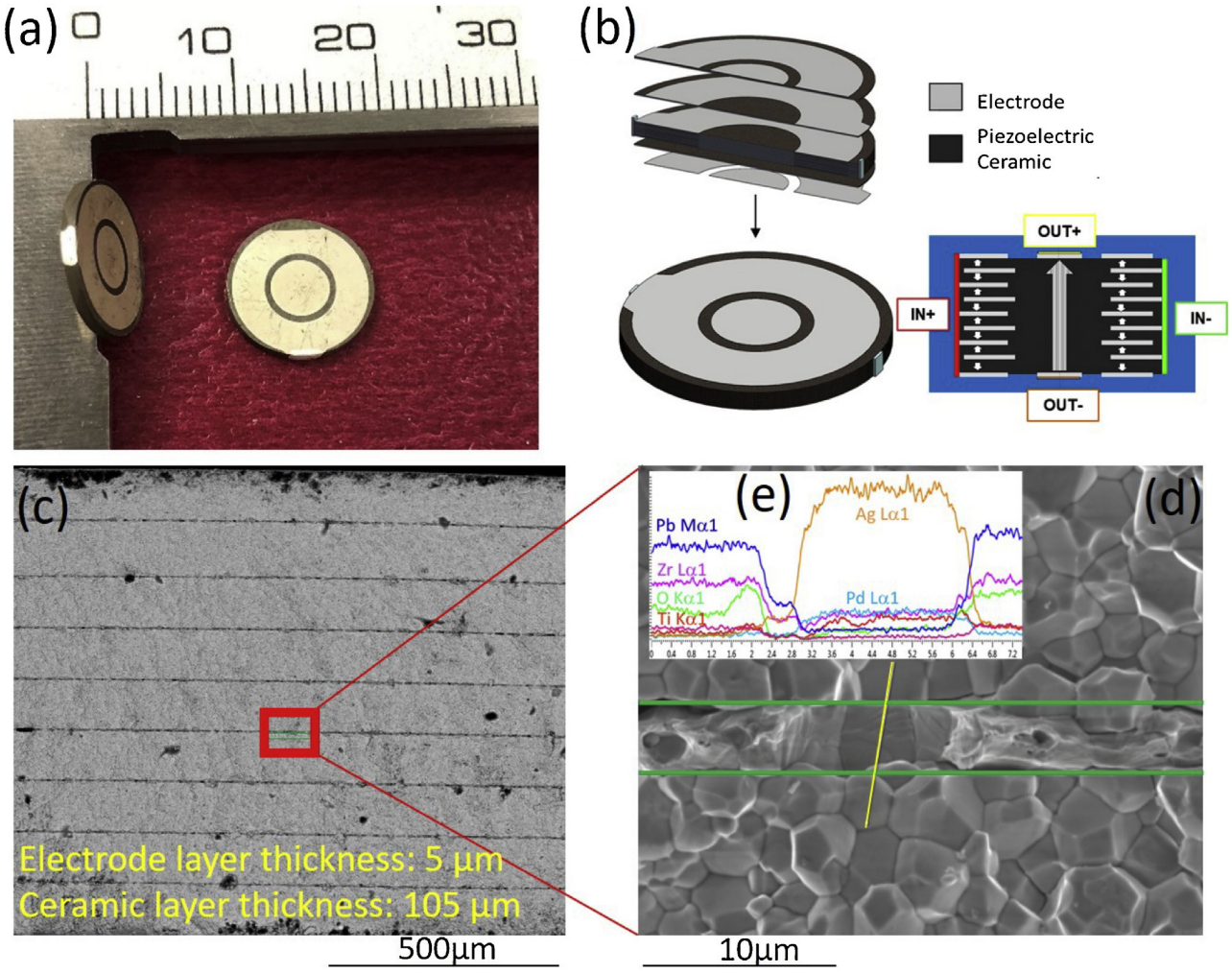

Fig. 9. A photo of the prototyped 10 mm OD, 1 mm thick PT (a) and poling directions and terminal connections (b) (top-left) view of the cofired layers of the ring-dot shape transformer, (bottom-right) polarization and electrical connections of transformer, (c) cross-sectional views from a fractured surface of the ring dot step up multilayer piezo transformer co-fired at 1000 °C for 2 h showing, (d) interface between ceramic grains and Ag/Pd fired electrode, and (e) EDS mapping around the ceramic-metal interface.

The degree of diffuseness, γ, changes from 1 to 2, where 1 represents the normal ferroelectric phase transition behaviour which obeys the Curie-Weiss law, and 2 refers to relaxor ferroelectric with diffuse phase transtion behaviour. The degree of diffuseness of PNN-PMW-PZT ceramics was calculated for different MnO_2 content by using Eq. (1), and found that γ value of an undoped ceramic changed from 1.45 to 1.33, 1.47 and 1.59 by doping 0.1, 0.25 and 0.5 wt% MnO_2, respectively. This indicated a diffuse ferroelectrics transition, as shown in Fig. 7. The relaxor phase transition of PNN-PMW-PZT ceramics can be associated with the diffuse phase transition and would be expected to give the composition with PNN and PMW phases.

Polarization - Electric field (P-E) curve and the electrical field induced bipolar strain hysteresis at 40 kV/cm of undoped PNN-PMW-PZT and 0.25 wt% MnO_2 doped PNN-PMW-PZT were provided in Fig. 8(a) and (b), respectively. Undoped PNN-PMW-PZT showed a saturated hysteresis loop with remanent polarization of 34.3 $\mu C/cm^2$. The typical butterfly loop reached ± 0.25% bipolar-strain by non 180° domain switching due to applied high field. Both the remanent polarization (12.05 $\mu C/cm^2$) and bipolar strain decreased in doped PNN-PMW-PZT due to the hardening effect by MnO_2 doping. The slightly pinched P-E curve and a non-symmetric bipolar-curve of the unpoled doped PNN-PMW-PZT can be explained with the defects dipole complex interactions with domain walls under applied electrical field [16]. In addition, defects and pinned or stabilized domains that were aligned with local polarization vector increased the internal bias (E_{int}) of 0.25 wt% MnO_2 doped unpoled PNN-PMW-PZT ceramic to 1.29 kV/cm. As expected, the undoped unpoled PNN-PMW-PZT ceramic has lower internal bias (E_{int} = 0.55 kV/cm) than doped ceramics [22]. Increase in internal bias is also supported by an increase in the mechanical Q, as shown in Fig. 4(a). Thus, the MnO_2 dopant content 0.25 wt% is more influential on the structure of the domain than the microstructure, which in turn determined hard piezoelectric properties that can be used for high power transformer application.

3.3. *Microstructural and electrical characterization of multilayer piezoelectric transformer*

A ring-dot type step-up piezoelectric transformer was prototyped from the modified PNN-PMW-PZT piezoceramic compositionto demonstrate the applicability of high power material properties in a device application. To achieve a large step-up ratio, the capacitance of primary (input) side should be considerably larger than the capacitance of the secondary (output) side. In order to obtain large input capacitance compared to output capacitance in a planar ring-dot type prototype, input (ring) side is constructed from thin piezoceramic layers with alternating polarization in thickness directions, thereby providing high capacitance, whereas the output (dot) side of the transformer is a uni-body with

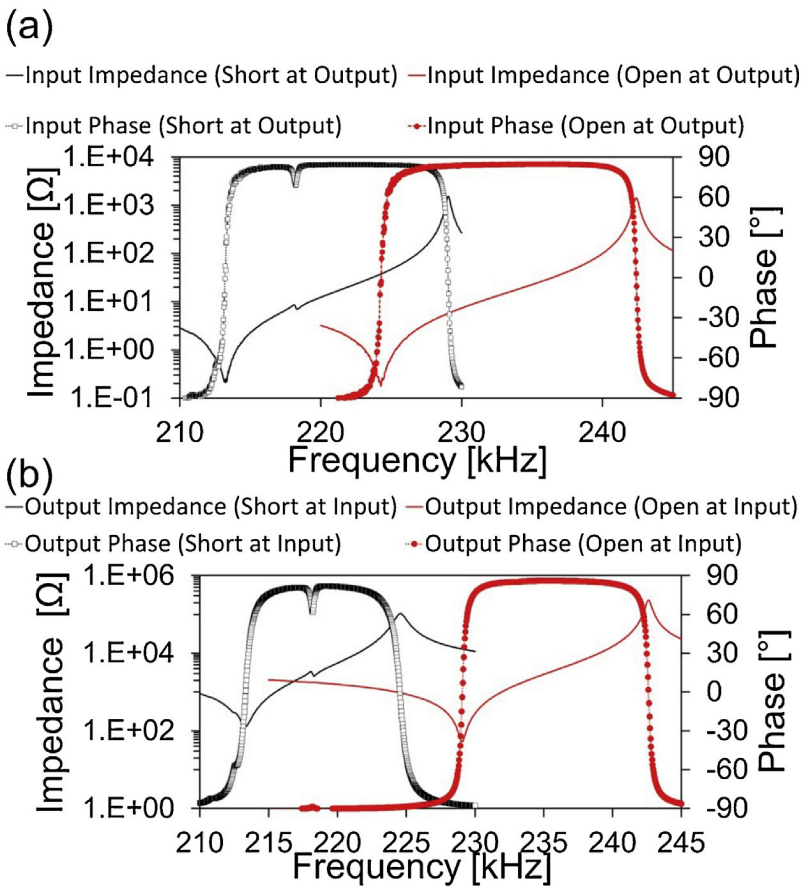

Fig. 10. Impedance and phase spectra of the input (a) and output (b) terminals of the devices for open and short circuit conditions.

significantly larger thickness (Fig. 9 (a)). After co-firing, the ratio of capacitance of the 3.6 mm wide multilayer ring-shape primary side (C_p = 42 nF) to the 5 mm dot-shape single layer secondary side (C_s = 280 pF) is 150, which is typical for planar type step-up PTs. Fig. 9(b) shows (top-left) exploded view of the cofired layers of the ring-dot shape transformer, (bottom-right) polarization and electrical connections. The prototyped PTs with new PMW composition showed dense microstructures without delamination, and ceramic-electrode interfaces were uniform, as shown in the SEM image of a fractured surface provided in Fig. 9. The ceramic and electrode layer thicknesses of PT were measured at 105 μm and 5 μm, respectively (Fig. 9(c)). The morphology of grains in the co-fired multilayer PTs in Fig. 9(d) is similar to the morphology of grains in bulk samples that were shown in Fig. (3), confirming the co-fired sintering conditions. The EDS mapping (Fig.9(e)) shows no interdiffusion between the metal electrode and ceramic layers and thus provides a clean metal-ceramic interface.

Electrical characterization of the devices includes small signal tests and high-power measurements. Small signal tests include the measurement of permittivity, and dielectric and mechanical losses, which provide important data to predict device characteristics. Capacitance and dielectric loss of the prototyped devices are measured with an LCR-meter (Sourcetronic ST2830) at 1 V, 1 kHz. Mechanical quality factor (Q_m) of the devices is calculated by using the 3-dB down method, which uses impedance spectrum data obtained by an HP-4395 A network analyzer. The impedance and phase spectrum of the input and output side of the PT at two extreme loading conditions (open and short) are showed in Fig. 10. The impedance and phase spectra provided in Fig. 10 show full polarization of the devices at both input and output sides as phase is larger than 80°. Fig. 10 also provides that the coupling coefficient of input side is larger than output side, as expected. In addition to the impedance-phase spectrum analysis at two extreme electrical loading cases, we also demonstrated the effect of electrical loading (resistance) on impedance and phase to represent similar conditions with high power measurements. Fig. 11 shows input phase (a) and impedance (b) spectrum of the device when output is connected to different loads. The dampening effect of the electrical load is clearly seen in impedance and phase plots of Fig. 11, as the device is loaded different than open circuit ($R_{load} = \infty$) and short circuit ($R_{load} = 0$) conditions. Optimum (matching) load is found to be 3 kΩ, where the damping effect is at maximum both on impedance and phase.

Although small signal (low power) analysis of devices establishes valuable information about the operating range (frequency and load) of PTs, high power analysis is the most critical characterization in terms of obtaining functional properties (power density and gain) and their deviation level at various high-power conditions. Due to the increased electric field, mechanical stress, and elevated temperature as a result of increased losses, material properties drift from room temperature values, which causes changes in device properties, such as the operating range, which can only be observed at application relevant high-power tests. During the high-power characterization of the piezoelectric transformers, devices are tested around their matching loads (~3 kΩ) when driven by sinusoidal (AC) input signal at operating frequencies between resonance (f_r) and anti-resonance (f_{ar}) of the fundamental mode, where the power efficiency (P_{out}/P_{in}) is maximized. Frequencies where the maximum gain and power are observed are illustrated by using an impedance-phase spectrum plot of an optimally loaded

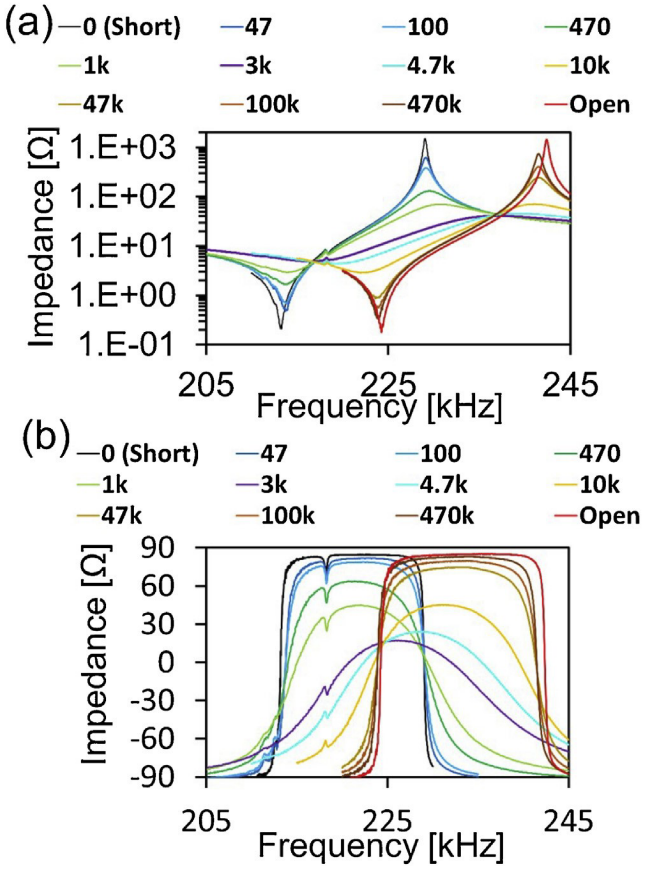

Fig. 11. The effect of electrical loading on the input impedance (a) and phase (b) as a function of the electrical loading at the output.

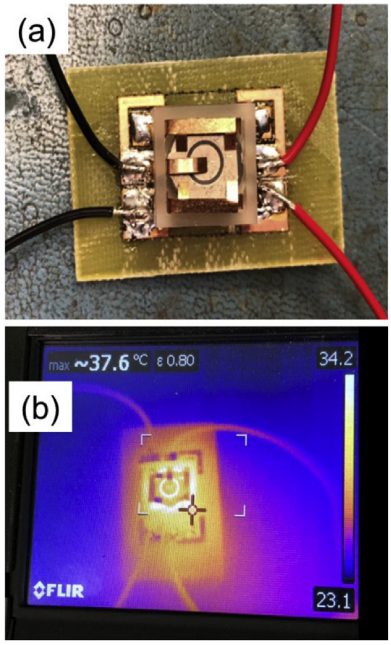

Fig. 13. The photo of a 10 mm-size device in spring loaded test package (a) and IR thermal image during high power tests (b).

device in Fig. 12 (a). Maximum gain is obtained around the resonance frequency (minimum impedance), and maximum efficiency is obtained around where phase is maximum at small signal (low power) tests. High power measurements were taken at specific output power (Pout) levels (e.g., 1 W, 2 W, 3 W) and limited with frequency range, as described above, to limit the maximum temperature increase (ΔT) of devices to only 40 °C. Fig. 12(b) shows the efficiency and associated temperature increase of the 10 mm OD, 1 mm thick (Volume = 78 mm^3) piezoelectric transformer when connected to its optimal load (3 kΩ) and providing 1, 2 and 3 W output, which corresponds to power densities of 12.7, 25.5, and 38.2 W/cm^3, respectively. Fig. 12(b) also shows that power density is directly related to the maximum allowable temperature increase from ambient temperature (ΔT), and thus higher power densities are achievable for higher ΔT. Further improvement of the power density of a piezoelectric transformer can come with suitable heat dissipating medium to drop the temperature to allowable limits. To achieve repeatable and standard measurements, the effect of conductive heat transfer to the test medium is minimized by inserting the piezoelectric transformers in a spring-loaded package with very small contact surface between the device and brass springs. The photo of a 10-mm size device in a spring-loaded package is shown in Fig. 13 (a), where the infrared thermal image of same device during test is shown in Fig. 13(b). Spring connection also provides electrical connection to the devices, which minimizes the clamping effect of solder wires in a typical device and thus improves the device performance.

Following the similar power characterization procedure provided in our previous paper [5], constant output power is provided by adjusting the input voltage for different resistive loads across the

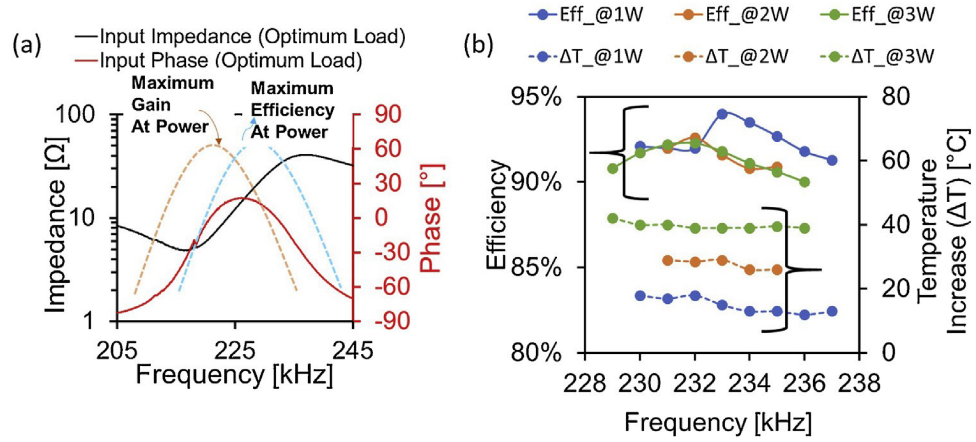

Fig. 12. The illustration of the gain and efficiency characteristics of an optimally loaded piezoelectric transformer shown with the small signal impedance and phase spectrum and phase spectrum (a), efficiency and temperature increase of piezoelectric transformers at 3kΩ as a function of operating frequency and output power (b).

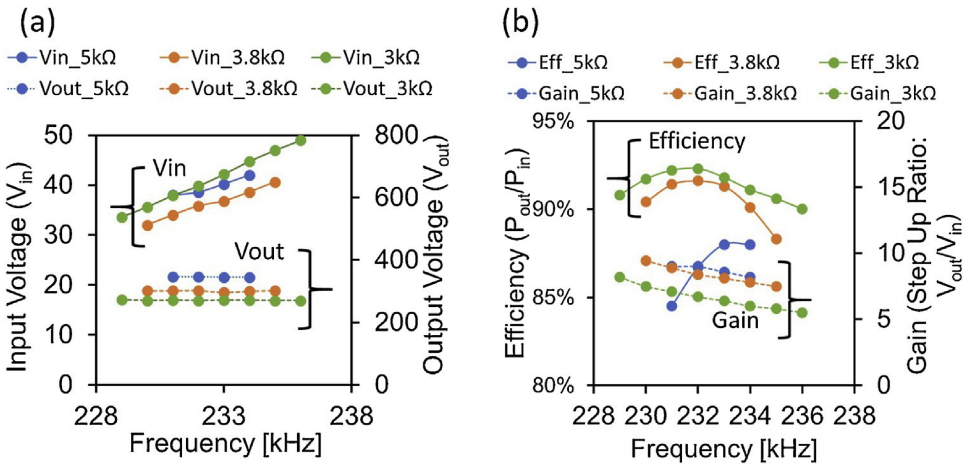

Fig. 14. Input and output voltage for constant power (3 W) output in a typical operation frequency range (a) and efficiency and gain at high power ($P_{d\text{-}out}$ = 38.2 W/cm^3) operation (b).

Table 1
Summary of step up piezoelectric transformers in the available literature based on their essential characteristics.

Reference	Material Type		T_{sinter} (°C)	Transformer Type	Power Density [W/cm3]	ΔT [°C]	Efficiency [%]	Gain
Yoo et al. 2001 [23].	PNW-PMN-PZT		–	Planar (Disk)	12.5	15.6	97	1.1
Laoratanakul et al. 2002 [24].	APC841		1280	Planar (Disk)	18.5	15	80	2.4
Priya et al. 2004 [4].	APC841		1280	Planar (Disk)	25.1	18	97	1.8
Lin et al. 2008 [25].	KNN		1100	Planar (Square)	10	20	96	6
Yang et al. 2011 [26].	NKN	Polycrystalline	1100	Planar (Disk)	18.3	3	94	3
Sun et al. 2015 [27].	NN-LT		1330	Planar (Disk)	32.8	27	92	4.5
					12.7	***13***	***94***	***6.7***
This Work	***PMW***		***1000***	***Planar (Disk)***	***25.5***	***29***	***93***	***6.7***
					38.2	***39***	***92***	***6.7***
Wang et al. 2016 [28]	PMN-PIN-PT		–	Rosen	50	5	95	1.2
Wang et al. 2008 [29]	PMN-PT	Single Crystal	–	Rosen	5.8	10	92	15
Zhuang et al. 2009 [30]	PMN-PT		–	Rosen	38	10	90	1.9

test frequency range. Fig. 14 (a) shows the increase in input voltage to keep output voltage constant at different electrical loads at constant output power (3 W). Efficiency and gain characteristics at 3 W (38.2 W/cm^3) output for different electrical loads around matching resistance is supported in Fig. 14(b) and found to be consistent with initial theoretical estimates provided in Fig. 12(a).

4. Conclusions

In this study, the development of a new, hard-piezoelectric ceramic composition for low temperature co-fired multilayer piezoelectric transformers is reported. A soft-type (Q_m = 50) PNN-PMW-PZT piezoceramic was successfully converted to a hard-type (Q_m = 1150) piezoelectric ceramic via MnO_2 additive, which was sintered at 1000 °C and exhibited excellent hard piezoelectric properties (Q_m = 1150, k_p = 0.63, tan δ: 0.0040, d_{33} = 350 pC/N, K = 1400, and T_C = 325 °C) for piezoelectric transformer applications. The new composition was co-fired with Ag/Pd inner electrodes in a planar-type, ring-dot multilayer step-up piezoelectric transformer, which demonstrated highest gain and power density compared to similar type piezoelectric transformers in the literature (See Table 1). The investigated disk shaped piezoelectric transformers, which have 1 mm thickness and 10 mm diameter, provided 6.7 step up ratio while delivering 3 W output power at 92% power efficiency, while the temperature increase from ambient is below 40 °C. The reported new hard-piezoceramic composition showed very prominent characteristics to be utilized in future low-temperature co-fired piezoelectric transformer developments.

Acknowledgements

This material is based upon work supported by the National Science Foundation [Grant No. 1632476]. Any opinions, findings, conclusions, or recommendations expressed in this material are those of the author(s) and do not necessarily reflect the views of the National Science Foundation.

Authors also would like to acknowledge Solid State Ceramics, Inc. employees: William Lock, Evan Babula, Ruchi Patel, and Addison Shableski and the Center for Dielectrics and Piezoelectric staff members: Joanne Aller, Amanda Baker, Jeffrey Long and Steven Perini for their technical support during this study.

References

[1] A. Vázquez Carazo, 50 years of piezoelectric transformers. Trends in the technology, MRS Proc. 785 (2003).
[2] J. Erhart, P. Půlpán, M. Pustka, Piezoelectric Ceramic Resonators, Chapter 5: Piezoelectric Transformers, Springer International Publishing Switzerland, ISSN 2364-3307, (2017), 155-203.
[3] A. Ochi, T. Inoue, S. Takahashi, Small multilayer piezoelectric transformers with high power density - characteristics of second and third-mode rosen-type transformers, Jpn. J. Appl. Phys. Part 1 Regul. Pap. Short Notes Rev. Pap. 38 (1999) 5598–5602.
[4] S. Priya, S. Ural, H.W. Kim, K. Uchino, T. Ezaki, Multilayered unipoled piezoelectric transformers, Jpn. J. Appl. Phys. Part 1 Regul. Pap. Short Notes Rev. Pap. 43 (2004) 3503–3510.
[5] A.E. Gurdal, S. Tuncdemir, K. Uchino, C.A. Randall, Low temperature co-fired multilayer piezoelectric transformers for high power applications, Mater. Des. 132 (2017) 512–517.
[6] S.Y. Yoo, J.Y. Ha, S.J. Yoon, J.W. Choi, High-power properties of piezoelectric hard materials sintered at low temperature for multilayer ceramic actuators, J. Eur. Ceram. Soc. 33 (2013) 1769–1778.

[7] D. Wan, Q. Li, J.-Y. Choi, J.-W. Choi, Y. Yang, S.-J. Yoon, Low-temperature sintered Pb(Zr,Ti)O $_3$–Pb(Mn,Sb)O_3–Pb(Zn,Nb)O_3 for multilayer ceramic actuators, Jpn. J. Appl. Phys. 49 (2010), 071503.
[8] J. Yoo, S. Lee, Piezoelectric properties of MnO2 doped low temperature sintering $Pb(Mn_{1/3}Nb_{2/3})O_3$–$Pb(Ni_{1/3}Nb_{2/3})O_3$–$Pb(Zr_{0.50}Ti_{0.50})O_3$ ceramics, J. Electroceramics. 23 (2008) 432–436.
[9] Q. Zhang, Y. Yue, R. Nie, H. Liu, Q. Chen, P. Yu, J. Zhu, D. Xiao, Achieving both high d_{33} and high T_C in low-temperature sintering $Pb(Ni_{1/3}Nb_{2/3})O_3$-$Pb(Mg_{1/2}W_{1/2})O_3$-$Pb(Zr_{0.5}Ti_{0.5})O_3$ ceramics using Li_2CO_3, Mater. Res. Bull. 85 (2017) 96–103.
[10] Y. Jeong, J. Yoo, S. Lee, J. Hong, Piezoelectric characteristics of low temperature sintering $Pb(Mn_{1/3}Nb_{2/3})O_3$-$Pb(Ni_{1/3}Nb_{2/3})O_3$-$Pb(Zr_{0.50}Ti_{0.50})O_3$ according to the addition of CuO and Fe_2O_3, Sens. Actuators A Phys. 135 (2007) 215–219.
[11] D.L. Corker, R.W. Whatmore, E. Ringgaard, W.W. Wolny, Liquid-phase sintering of PZT ceramics, J. Eur. Ceram. Soc. 20 (2000) 2039–2045.
[12] C.A. Randall, A. Kelnberger, G.Y. Yang, R.E. Eitel, T.R. Shrout, High strain piezoelectric multilayer Actuators–A material science and engineering challenge, J. Electroceramics. 14 (2005) 177–191.
[13] N.J. Donnelly, T.R. Shrout, C.A. Randall, The role of Li_2CO_3 and PbO in the low-temperature sintering of Sr, K, Nb (SKN)–doped PZT, J. Am. Ceram. Soc. 92 (2009) 1203–1207.
[14] Y. Yan, H. He, Y. Feng, Effect of MnO_2 addition on the electrical properties of PNZST ceramics, J. Electron. Mater. 43 (2014) 1460–1465.
[15] T.M. Kamel, G. de With, Poling of hard ferroelectric PZT ceramics, J. Eur. Ceram. Soc. 28 (2008) 1827–1838.
[16] B.S. Li, G.R. Li, Q.R. Yin, Z.G. Zhu, A.L. Ding, W.W. Cao, Pinning and depinning mechanism of defect dipoles in PMnN-PZT ceramics, J. Phys. D. Appl. Phys. 38 (2005) 1107–1111.
[17] C.A. Randall, A.D. Hilton, D.J. Barber, T.R. Shrout, Extrinsic contributions to the grain size dependence of relaxor ferroelectric $Pb(Mg_{1/3}Nb_{2/3})O_3$: $PbTiO_3$ ceramics, J. Mater. Res. 8 (1993) 880–884.
[18] S. Zhang, N.P. Sherlock, R.J. Meyer, T.R. Shrout, Crystallographic dependence of loss in domain engineered relaxor-PT single crystals, Appl. Phys. Lett. 94 (2009).
[19] S.M. Lee, S.H. Lee, C.B. Yoon, H.E. Kim, K.W. Lee, Low-temperature sintering of MnO_2-doped PZT-PZN piezoelectric ceramics, J. Electroceramics. 18 (2007) 311–315.
[20] S. Zhang, R. Xia, L. Lebrun, D. Anderson, T.R. Shrout, Piezoelectric materials for high power, high temperature applications, Mater. Lett. 59 (2005) 3471–3475.
[21] N. Vittayakorn, G. Rujijanagul, X. Tan, M.A. Marquardt, D.P. Cann, The morphotropic phase boundary and dielectric properties of the $xPb(Zr_{1/2}Ti_{1/2})O_3$-(1-x)$Pb(Ni_{1/3}Nb_{2/3})O_3$ perovskite solid solution, J. Appl. Phys. 96 (2004) 5103–5109.
[22] S. Zhang, S.-M. Lee, D.-H. Kim, H.-Y. Lee, T.R. Shrout, Characterization of Mn-modified $Pb(Mg_{1/3}Nb_{2/3})O_3$–$PbZrO_3$–$PbTiO_3$ single crystals for high power broad bandwidth transducers, Appl. Phys. Lett. 93 (2008), 122908.
[23] J. Yoo, K. Yoon, S. Hwang, S. Suh, J. Kim, C. Yoo, Electrical characteristics of high power piezoelectric transformer for 28W fluorescent lamp, 90 (2000) 132–137.
[24] P. Bouchilloux, K. Uchino, Unipoled disk-type piezoelectric transformers, Jpn. J. Appl. Phys. Part 1 Regul. Pap. Short Notes Rev. Pap. 41 (2002) 1446–1450.
[25] D. Lin, M.S. Guo, K.H. Lam, K.W. Kwok, H.L.W. Chan, Lead-free piezoelectric ceramic $(K_{0.5}Na_{0.5})NbO_3$ with MnO_2 and $K_{5.4}Cu_{1.3}Ta_{10}O_{29}$ doping for piezoelectric transformer application, Smart Mater. Struct. 17 (2008) 35002.
[26] S.L. Yang, C.C. Tsai, Y.C. Liou, C.S. Hong, B.J. Li, S.Y. Chu, Effects of improved process for CuO-doped NKN lead-free ceramics on high-power piezoelectric transformers, IEEE Trans. Ultrason. Ferroelectr. Freq. Control. 58 (2011) 2555–2561.
[27] H.L. Sun, D.M. Lin, K.H. Lam, M.S. Guo, S.H. Choy, K.W. Kwok, H.L.W. Chan, High power density $NaNbO_3$-$LiTaO_3$ lead-free piezoelectric transformer in radial vibration modes, Smart Mater. Struct. 24 (2015) 1–8.
[28] Q. Wang, C. Ma, F. Wang, B. Liu, J. Chen, H. Luo, T. Wang, W. Shi, Note: High-power piezoelectric transformer fabricated with ternary relaxor ferroelectric $Pb(Mg_{1/3}Nb_{2/3})O_3$–$Pb(In_{1/2}Nb_{1/2})O_3$–$PbTiO_3$ single crystal, Rev. Sci. Instrum. 87 (2016), 036105.
[29] F. Wang, W. Ge, P. Yu, X. Zhao, H. Luo, Y. Zhang, J. Wu, Multilayer rosen-type piezoelectric transformer prepared with $Pb(Mg_{1/3}Nb_{2/3})O_3$–$PbTiO_3$ single crystal, J. Phys. D. Appl. Phys. 41 (2008), 035409.
[30] Y. Zhuang, S.O. Ural, R. Gosain, S. Tuncdemir, A. Amin, K. Uchino, High power piezoelectric transformers with $Pb(Mg_{1/3}Nb_{2/3})O_3$–$PbTiO_3$ single crystals, Appl. Phys. Express. 2 (2009), 121402.

Biographies

Sinan Dursun is a Post-Doctoral Researcher of Materials Research Institute at The Pennsylvania State University. He received the B.Sc. degree in Physics from Ege University, Turkey (2007). He has a Ph.D. in Materials Science and Engineering from Gebze Technical University, Turkey (2017) where worked as a research assistant between 2012 and 2017. His main research interests include multi-layer prototyping, powder processing, cold sintering processing (CSP), textured piezoceramics, FEA design, actuators. He is an author or co-author of 15 papers and a patent pending.

A. Erkan Gurdal is the Chief Technology Officer at Solid State Ceramics, Inc. in State College, PA, USA. He has a B.Sc. in Metallurgical & Materials Engineering from Istanbul Technical University, Turkey (2009), and a Ph.D. in Materials Science and Engineering from The Pennsylvania State University, USA (2014). His research interests include compositional development of piezoceramics, thick-film multilayer prototyping, FEA design, and characterization methodologies of piezoelectric device performance.

Safakcan Tuncdemir is the President of Solid State Ceramics, Inc., a start-up in advanced piezoelectric materials and devices. He has a B.Sc and M.Sc in Mechanical Engineering with focus on Mechatronics from Middle East Technical University, Turkey (2002 and 2005). He also holds a Ph.D. in Electrical Engineering on multifunctional piezoelectric actuators from The Pennsylvania State University, USA (2011), where worked as a researcher between 2005 and 2012. Since he joined Solid State Ceramics, he has been developing high power high performance multilayer piezoelectric devices for various applications. He authored 18 papers and a patent.

Clive A. Randall is Professor of Materials Science and Engineering and Director of Materials Research Institute at The Pennsylvania State University. He has a B.Sc. (Honors) in Physics from University of East Anglia, UK (1983), and a Ph.D. in Experimental Physics from University of Essex, UK (1987). He was Director for the Center for Dielectric Studies 1997–2013, and Co-Director of the Center for Dielectrics and Piezoelectrics 2013–2015 (now Technical Advisor). Interests include discovery, processing, material physics, and compositional design of functional materials. Among his awards are Fellow of the American Ceramic Society and Academician of World Academy of Ceramics.